19

Progress Research on Wireless Communication Systems for Underground Mine Sensors

Larbi Talbi[1], Ismail Ben Mabrouk[1] and Mourad Nedil[2]
[1]*Université du Québec en Outaouais*
[2]*Université du Québec en Abitibi-Témiscamingue*
Canada

1. Introduction

After a recent series of unfortunate underground mining disasters, the vital importance of communications for underground mining is underlined one more time. Establishing reliable communication is a very difficult task for underground mining due to the extreme environmental conditions. Nevertheless, wireless sensors are considered to be promising candidates for communication devices for underground mine environment. Hence, they can be useful for several applications dealing with the mining industry such as Miners' tracking, prevention of fatal accident between men and vehicles, providing warning signals when miner entering the unsafe area, monitoring underground gases, message communication, etc.

Despite its potential advantages, the realization of wireless sensors is challenging and several open research problems exist. In fact, underground communication is one of the few fields where the environment has a significant and direct impact on the communication performance. Furthermore, underground mines are very dynamic environments. As mines expand, the area to be covered expands automatically.

In mine, communication requires complete coverage inside the mine galleries, increasing system reliability and higher transmission rates for faster data throughput. It is extremely important for information to be conveyed to and gathered from every point of mine due to both safety and productivity reasons. In order to meet these needs, the communications industry has looked to Ultra-Wide-band (UWB) for wireless sensors. There have been numerous research results in the literature to indicate that UWB is one of the enabling technologies for sensor network applications [1, 2, 3, 4, 5, 6]. Therefore, UWB provides a good combination of high performance with low complexity for WSN applications [7, 8, 9, 10].

Since UWB has excellent spatial resolution it can be advantageously applied in the field of localization and tracking [11, 12, 13]. In addition to UWB technology, multiple antenna systems have drawn great interest in the wireless community. Multiple antenna systems employ multiple antennas at the transmitter, receiver, or both. By using the antennas in a smart fashion, it may be possible to achieve array gain or diversity gain when multiple antennas are located at either the transmitter or receiver link ends. When multiple antennas are present at both link ends, however, the achievable data rate can potentially be increased linearly proportional to the minimum of the number of antennas at the link ends.

In a sensor network, nodes are generally densely deployed. They do not compete with each other but collaborate to perform a common task. Consider a situation where multiple nodes sense the same object and feed the measurements to a remote data fusion center (relay station). Since nodes are spatially clustered, it is natural to let them cooperate as multiple inputs in transmission and receiving, for the ultimate objective to save energy. In [14], Cui, Goldsmith and Bahai investigated the energy efficiency of MIMO and cooperative MIMO techniques in sensor networks. They mainly consider using MIMO for diversity gain, which improves the quality of the link path.

This chapter will study the application of UWB and MIMO techniques in wireless sensor networks. Hence, a channel characterization of the wireless underground channel is essential for the proliferation of communication protocols for wireless sensor network.

2. UWB channel characterization

2.1 Description of the underground mining environment

The measurements were performed in various galleries of a former gold mine, at a 70 m underground level. The environment mainly consists of very rough walls and the floor is not flat and it contains some puddles of water. The dimension of the mine corridors varies between 2.5 m and 3 m in width and approximately 3 m in high. The measurements were taken in both line of sight (LOS) and non line of sight (NLOS) scenarios. Figure 1 illustrates photography of the underground gallery and the measurement arrangement.

Fig. 1. Photography of the Underground Gallery and the Measurement Arrangement.

2.2 Measurement campaign

The transmitter antenna was always located in a fixed position, while the receiver antenna was moved throughout along the gallery on 49 grid points. As shown in figure 2, the grid was arranged as 7X7 points with 5 cm spacing between each adjacent point. The 5

centimetres corresponds to half of wavelength of the lowest frequency component for uncorrelated small scale fading. During all measurements, the heights of the transmitting and receiving antennas were maintained at 1.7 m in the same horizontal level, and the channel was kept stationary by ensuring there was no movement in the surrounding environment.

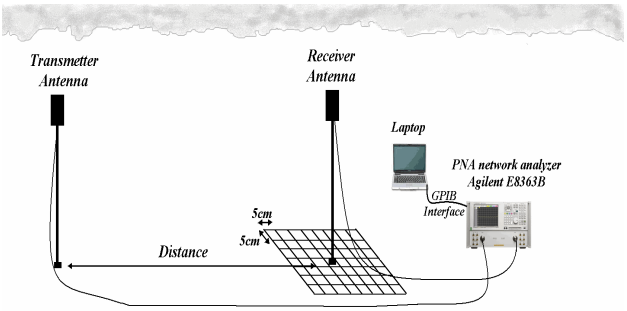

Fig. 2. Overview of the Measurement Setup

The UWB measurements were performed in frequency domain using the frequency channel sounding technique based on S21 parameter obtained with a network analyzer. In fact, the system measurement setup consists of E8363B network analyzer (PNA) and two different kinds of antennas, with directional and omnidirectional radiation patterns, respectively. There were no amplifiers used during the measurements because the distance between the transmitter and the receiver was just 10 meters. The transmitting port of the PNA swept 7000 discrete frequencies ranging from 3 GHz to 10 GHz uniformly distributed over the bandwidth, and the receiving port measured the magnitude and the phase of each frequency component. Figure 3 shows a typical complex channel transfer function (CTF) measured with the Network Analyzer.

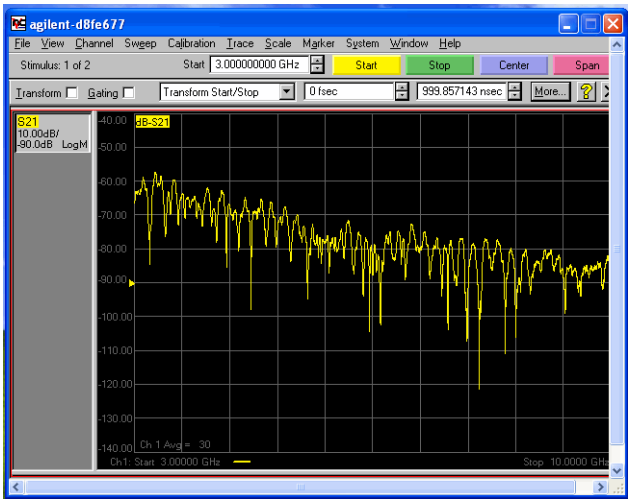

Fig. 3. Channel Transfer Function Measured with the Agilent E8363B Network Analyzer

The frequency span of 1 MHz is chosen small enough so that diffraction coefficients, dielectric constants, etc., can be considered constant within the bandwidth of 7 GHz [15]. At each distance between the transmitter and the receiver, the channel transfer function was measured 30 times, to reduce the effects of random noise on the measurements, and then stored in a computer hard drive via a GPIB interface. The 7 GHz bandwidth gives a theoretical time resolution of 142.9 ps (in practice, due to the use of windowing the time resolution is estimated to be 2/bandwidth) and the sweeping time of the network analyzer is decreased to validate the quasi- static assumption of the channel. The frequency resolution of 1 MHz gives maximum delay range of 1 μs.

Before the measurements, the calibration of the setup was done to reduce the influence of unwanted RF cables effects. Table 1 lists the parameters setup.

Parameters	**Values**
Bandwidth	7 GHz
Center Frequency	6.5 GHz
Frequency Sweeping Points	7000
Frequency Resolution	1 MHz
Time Resolution	286 *ps*
Maximum Delay Range	1000 *ns*
Sweep Average	30
Tx-Rx Antennas Height	1.7 m

Table 1. Measurement System Parameters

Since the measurements are performed in frequency domain, the inverse Fourier transform (IFT) was applied to the measured complex transfer function using Kaiser-Bessel window in order to obtain the channel impulse response. The Kaiser window is designed as FIR filter with parameter β=6 to reduce the side lobes of the transformation.

2.3 Measurements results and analysis

The large scale measurements are performed to determine the propagation distance-power law in the underground environment. The average path loss in dB for arbitrary transmitter-receiver separation distance d can be represented as:

$$PL_{average}(d) = \frac{1}{M}\frac{1}{N}\sum_{i=1}^{M}\sum_{j=1}^{N}\left|H(f_i, d)\right|^2 \tag{1}$$

where H(f_i,d) is the measured complex frequency response and N represents the number of data points measured during a sweep of 7000 discrete frequencies ranging from 3 GHz to 10 GHz, and M represents the number of sweeps that has been averaged.

According to the measured channel transfer function and the data fitting using the linear least squares regression, the computations of different transmitter-receiver antennas

combination have shown that the path loss PL (d) in dB at any location in the gallery can be written as a random log-normal distribution by :

$$PL_{dB}(d) = PL_{dB}(d_0) + 10.n.\log_{10}\left(\frac{d}{d_0}\right) + X_\sigma \quad (2)$$

where PL(d_0) is the path loss at the reference distance d_0 set to 1m, n is the path loss exponent and X_σ is a zero-mean Gaussian distributed random variable in dB with the standard deviation.

2.3.1 LOS scenario

2.3.1.1 Path loss model

The measurements of UWB propagations channel in line of sight case were made between 1 m and 10 m with intervals of 1 m. Figure 4 illustrates the gallery layout and the measurements Tx-Rx arrangements under LOS and Figure 5 shows the results of path loss as function of distance for the three antennas combinations: directional - directional, directional-omni and omni-omni.

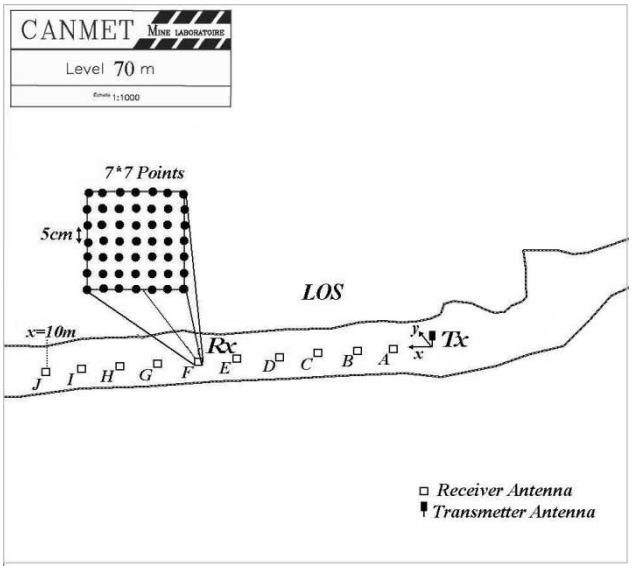

Fig. 4. Gallery Layout and Measurement Setup in LOS

As listed in Table 2, the path loss exponent n, in LOS scenario is equal to 1.99, 2.01 and 2.11 for directional-omni, directional-directional, and omni-omni antennas combination respectively. It can be noted that the path loss exponent for all these combinations is close to free space path loss exponent where n=2, with the smallest path loss fluctuation for directional-omni antenna combination, and the standard deviation of Gaussian random variable σ_{dB} is smaller for directional antenna in LOS environment. The results of path loss exponent values observed in [16] [17] for indoor UWB propagation are lower to the results

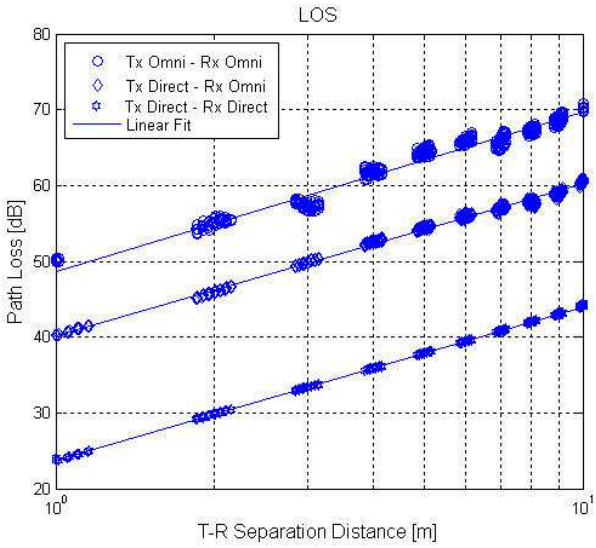

Fig. 5. Path Loss vs. T-R Separation Distance in LOS

obtained for underground UWB propagation. In an indoor environment, such as a corridor or a hallway clear of obstacles, the results may show lower path loss exponent due to multipath signal addition, whereas in the mine gallery, the walls are uneven, scattering the signal and thus showing results in closer agreement with the free-space path loss exponent, due mainly to the LOS component reaching the antenna.

LOS	*Omni – Omni*	*Direct – Direct*	*Direct – Omni*
n	2.11	2.01	1.99
σ_{dB}	0.89	0.13	0.32

Table 2. Summary of Path Loss Exponents n and Standards Deviations σ_{dB} in LOS.

2.3.1.2 RMS delay spread

A statistical characterization of the channel impulse response is a useful process for describing the rapid fluctuations of the amplitude, phase, and multipath propagation delays of the UWB signal. The number of multipath in an underground environment is more important due to the reflection and scattering from the ground and surrounding rough surfaces. Figure 6 shows a typical power delay profile (PDP) measured with omni-omni antenna in LOS environment.

In order to compare different multipath channels of different antennas combination, the mean excess delay and RMS delay spread are evaluated using the below equations [18] :

- RMS delay spread is the square root of the second central moment of the power delay profile given by:

$$\tau_{rms} = \sqrt{\overline{\tau^2} - \left(\overline{\tau}\right)^2} \tag{3}$$

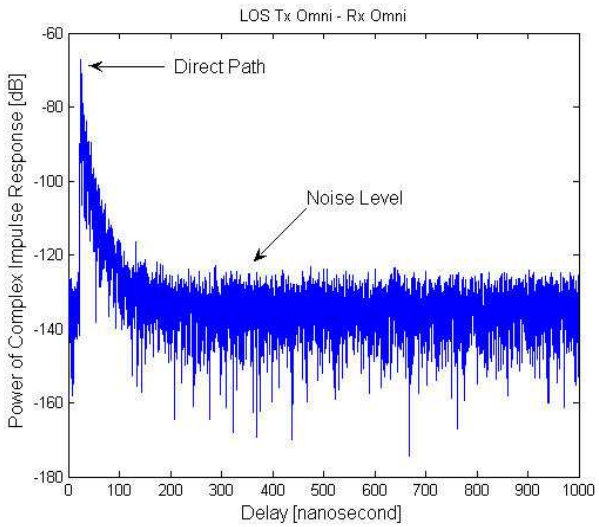

Fig. 6. Typical underground Power Delay Profile in LOS

- Mean excess delay is the first moment of the power delay profile defined by:

$$\overline{\tau} = \frac{\sum_k a_k^2.\tau_k}{\sum_k a_k^2} = \frac{\sum_k P(\tau_k).\tau_k}{\sum_k P(\tau_k)} \tag{4}$$

$$\overline{\tau^2} = \frac{\sum_k a_k^2.\tau_k^2}{\sum_k a_k^2} = \frac{\sum_k P(\tau_k).\tau_k^2}{\sum_k P(\tau_k)} \tag{5}$$

Where a_k, $P(\tau_k)$ and τ_k are the gain, power and delay of the k^{th}path respectively. From (3), (4) and (5) we have calculated the RMS delay spread for each antenna combination by using predefined thresholds. A threshold of 40 dB below the strongest path was chosen to avoid the effect of noise on the statistics of multipath arrival times. Fig. 7 shows the effects of antenna directivity on the RMS delay spread computed from the cumulative distribution function in LOS scenario.

According to the figure 7, we can observe that for 50% of all locations, the directional - directional combination offers the best result of τ_{rms} with 2 ns. However, the directional-omni and the omni-omni combinations introduce 7.7 ns and 9.5 ns of τ_{rms} respectively. Hence, we can say that the former combination reduces 7.5 ns of τ_{rms} in comparison with the latter one. The effect of directional antenna in underground LOS environment is similar to the results reported in indoor channel [19] [20].

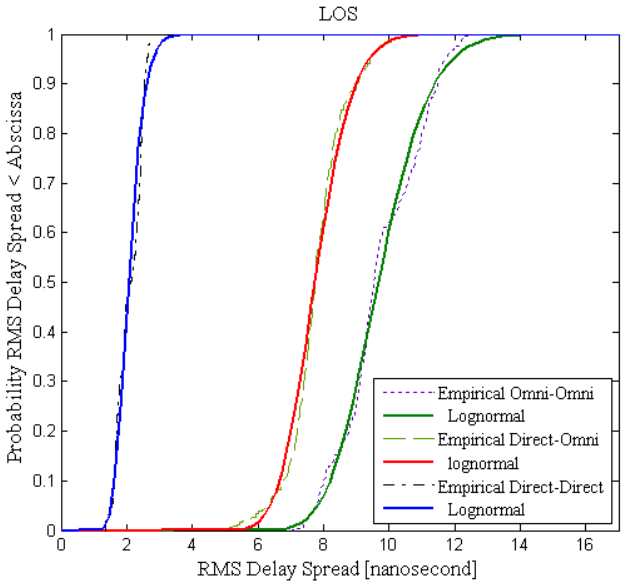

Fig. 7. Cumulative Distribution Function of RMS delay spread in LOS

2.3.2 NLOS scenario

2.3.2.1 Path loss model

The measurements of UWB propagations in non line of sight were made between 4 m and 10 m with intervals of 1m. Figure 8 illustrates the gallery layout and the measurements arrangement in NLOS.

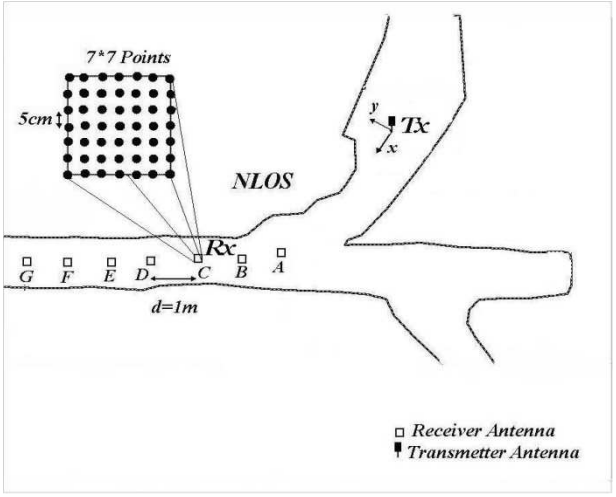

Fig. 8. Gallery Layout and Measurement Setup in NLOS

The results of path loss as function of distance for directional - directional and omni - omni antennas combinations are shown in Figure 9.

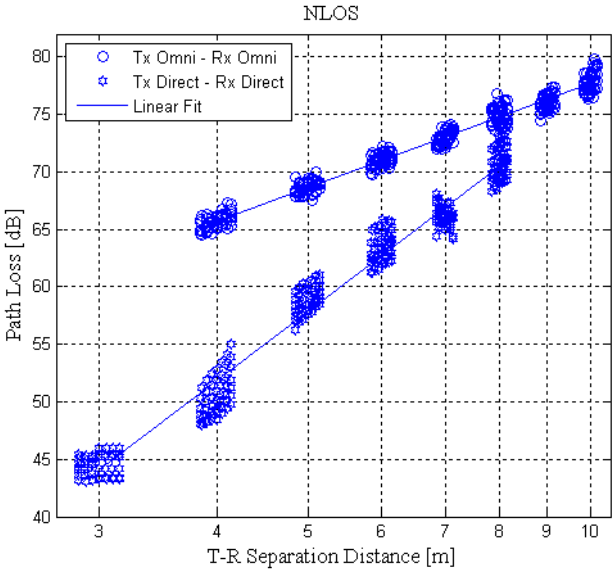

Fig. 9. Path Loss vs. T-R Separation Distance in NLOS

As listed in Table 3, the path loss exponent with directional antennas is twice larger than of the omnidirectional antennas.

NLOS	*Omni – Omni*	*Direct – Direct*
n	3.00	6.16
σ_{dB}	0.66	1.47

Table 3. Summary of Path Loss Exponents n and Standards Deviations σ_{dB} in NLOS

2.3.2.2 RMS delay spread

In NLOS scenario, the UWB signal reaches the receiver through reflections, scattering, and diffractions. Figure 10 shows that a typical power delay profile (PDP) measured with Omni-Omni antenna in NLOS environment consists of components from multiple reflected, scattered, and diffracted propagation paths.

Figure 11 shows that the use of directional antennas, for 50% of all locations in NLOS scenario, can reduce, 13 ns of τ_{rms} compared to omnidirectional antennas.

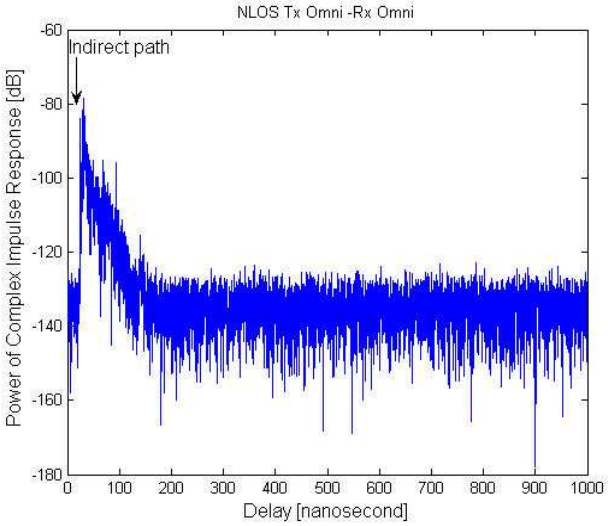

Fig. 10. Path Loss vs. T-R separation distance in NLOS

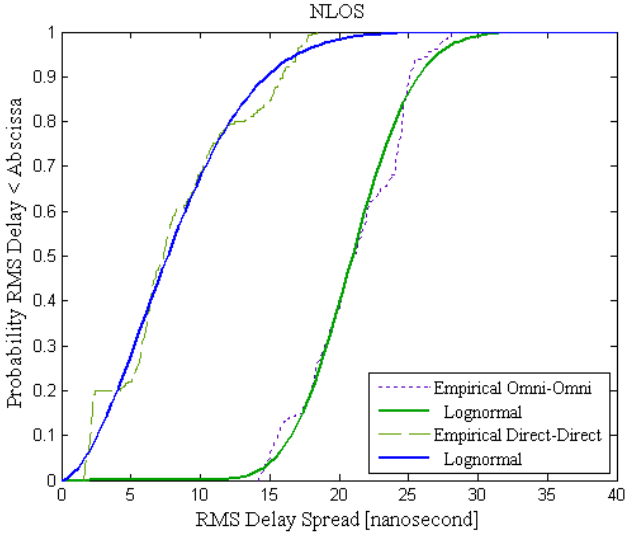

Fig. 11. Cumulative Distribution Function of RMS delay spread in NLOS

3. MIMO channel characterization at 2.4 GHz

3.1 Description of the underground environment

Measurements were conducted in a gallery located at a 40-m deep underground level.

In this gallery, the floor is uneven with bumps and several ditches. In addition, the walls are not aligned. Dimensions vary almost randomly throughout the gallery, although the latter is

supposed to have a width of about 4 to 5 m. The gallery also has several branches of different size at variant locations. The humidity is still high, drops of water falling from everywhere and big pools of water cover the ground. The temperature is stable of 6 to 15º C along the year. A photography of this underground gallery is shown in figure 12.

Fig. 12. Photography of the mine gallery

3.2 Measurement setup

The MIMO antenna system consists of a set patch antenna, developed in our laboratory and have been used for transmission and reception of the RF signal, at 2.4GHz. Measurement campaigns under LOS and NLOS scenarios were performed in frequency domain using the frequency channel sounding technique based on measuring S_{21} parameter with a network analyzer (Agilent E8363B). In fact, the system measurement setup, as shown in figure 13, consists of a network analyzer (PNA), 2X2 MIMO antenna set, two switches, one power amplifier for the transmitting signal and one low noise amplifier for the receiving signal. Both amplifiers have a gain of 30 dB.

For the Line-of-Sight (LOS) scenario, the transmitter remained fixed at T_{x1} , where the receiver changed its position along the gallery, from 1 meter up to 25 meters far from the transmitter. While for NLOS the transmitter remained fixed at T_{x2} and the $T_x - R_x$ separation varies from 6m up to 25m. Figure 14 illustrates photography of the receiver location and a map of the underground gallery.

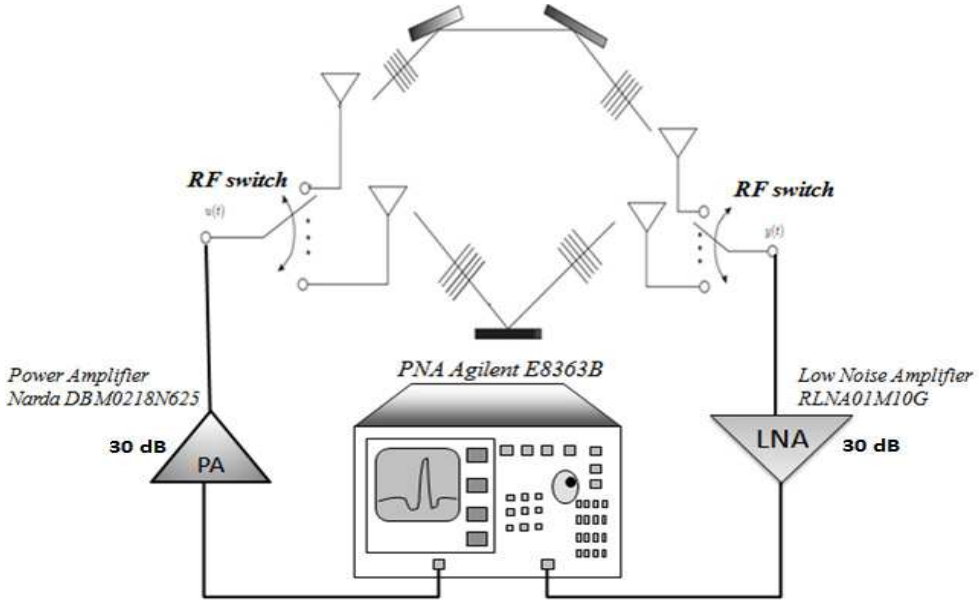

Fig. 13. Measurement setup

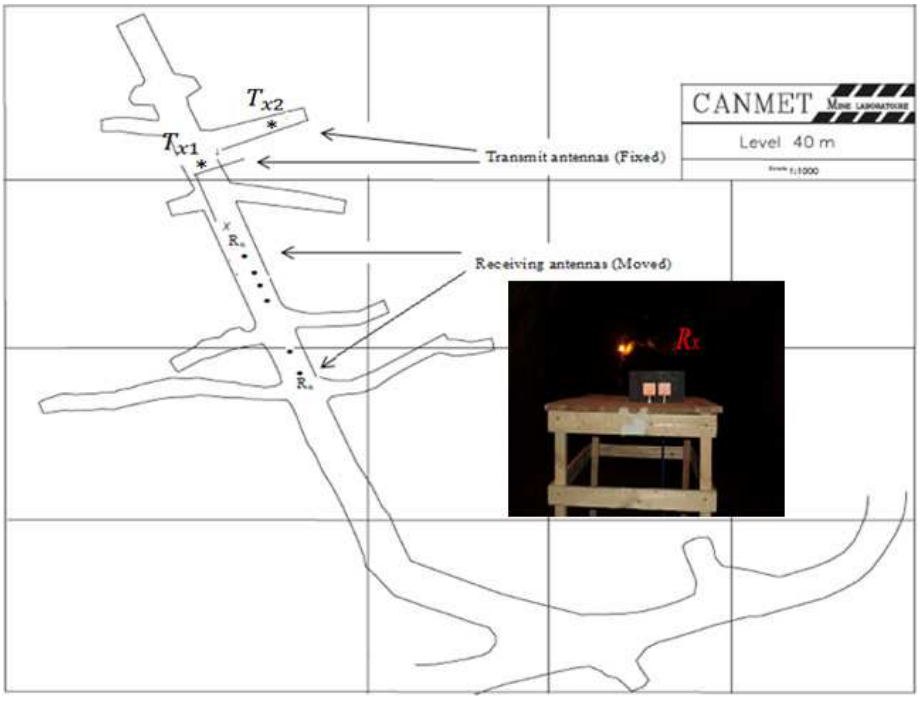

Fig. 14. The underground gallery plan

3.3 Measurement results

3.3.1 RMS delay (τ_{RMS})

The RMS delay spread roughly characterizes the multipath propagation in the delay domain. The RMS delay spread is the square root of the second central moment of the averaged power and it is defined as:

$$\tau_{rms} = \sqrt{\overline{\tau^2} - (\overline{\tau})^2} = \sqrt{\frac{\sum_i P_i \tau_i^2}{\sum_i P_i} - \left(\frac{\sum_i P_i \tau_i}{\sum_i P_i}\right)^2} \quad (6)$$

where $\bar{\tau}$ is the mean excess delay, $\overline{\tau^2}$ is the average power and P_i is the received power (in linear units) at τ_i corresponding arrival time. We have a threshold of 10 dB for all power delay profiles, in order to guarantee the elimination of the noise.

The RMS delay spread has been computed for each impulse response of all the gallery measurements using the 2X2 MIMO system under LOS and NLOS scenarios and plotted in terms of the separation distance d_{Tx-Rx} in figure 15.

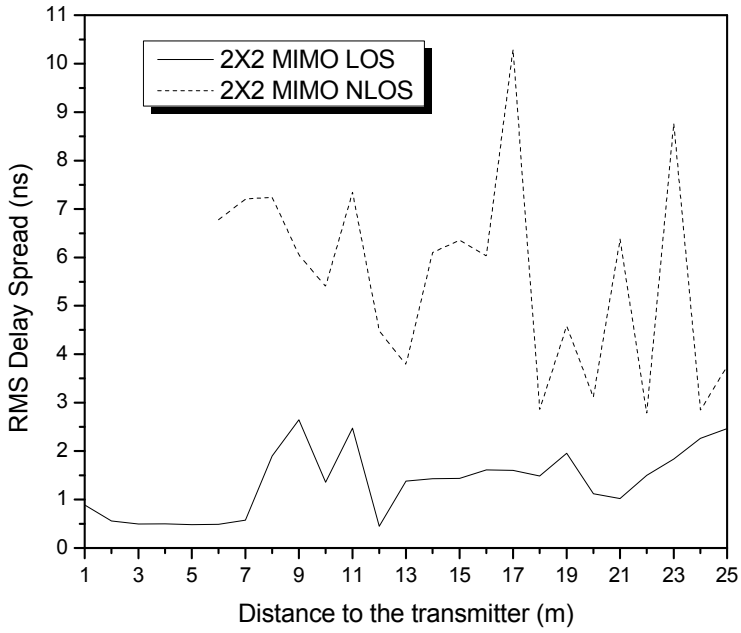

Fig. 15. RMS delay spread as a function of the distance

For the considered underground gallery, the profile seen in figure 15 is not monotonically increasing as may be expected. Results thus show propagation behavior that is specific for these underground environments. This is likely due to scattering on the rough sidewalls' surface that exhibit a difference of 25 cm between the maximum and minimum surface variation. Moreover, the RMS delay for the MIMO in NLOS scenario is higher than the one

of MIMO by about 5 ns due to the walls attenuation. Table 4 summarizes the RMS values for LOS and NLOS locations.

RMS (ns)	MIMO LOS	MIMO NLOS
Minimum / Maximum	0.44 / 2.64	2.7815 / 10.292
Mean / Standard deviation (σ)	1.33 / 0.68	5.6081 / 2.0750

Table 4. Summary of the RMS delay spread for measurements corresponding to LOS and NLOS galleries

3.3.2 Path loss

Path loss in the channel is normally distributed in decibel (dB) with a linearly increasing mean and is modeled as:

$$PL_{dB}(d_0) = \overline{PL_{dB}}\ (d_0) + 10\alpha\log\ (\frac{d}{d_0}) + X \tag{7}$$

where $\overline{PL_{dB}}\ (d_0)$ is the mean path loss at the reference distance d_0, $10\alpha\log\ (d/d_0)$ is the mean path loss referenced to d_0, and X is a zero mean Gaussian random variable expressed in dB. Path Loss as a function of distance are shown in figure 16 and figure 17 for both LOS and NLOS galleries respectively. The mean path loss at d_0 and the path loss exponent α were determined through least square regression analysis [21]. The difference between this fit and the measured data is represented by the Gaussian random variable X. Talble 5 lists the values obtained for α and σ_X (standard deviation of X).

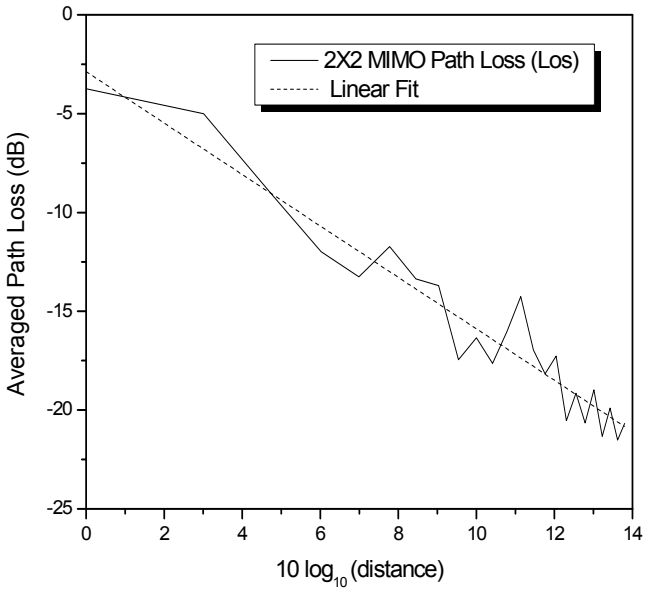

Fig. 16. Average Path versus distance in LOS scenario

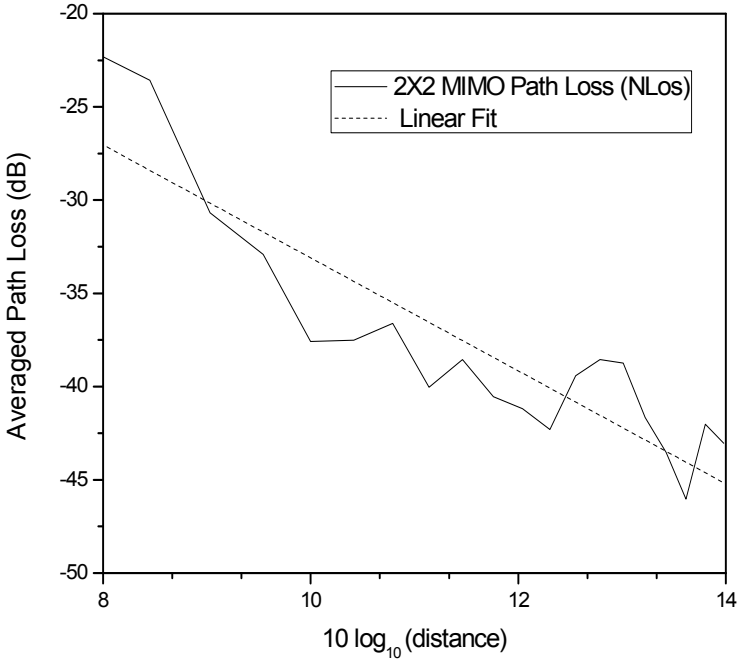

Fig. 17. Average Path versus distance in NLOS scenario

	MIMO LOS	MIMO NLOS
α	1.73	3.03
σ_X	1.29	2.75

Table 5. Path Loss exponent α and standard deviation of X (σ_X)

From the results shown in Table 5 the NLOS scenario have path loss exponent greater than 2 and also have larger σ_X value compared with LOS scenarios. While, for the LOS case the exponent α=1.73, is smaller than the free space exponent α=2, the reason behind this is because of the collection of all multipath components so that a higher power is received than the direct two signals in the free space.

3.3.3 Capacity

If we consider a system composed on m transmitting antennas and n receiving antennas, the maximum capacity of a memoryless MIMO narrow band channel expressed in bits/s/Hz, with a uniform power allocation constraint and in the presence of additional white Gaussian noise is given by Foschini et al.[22]:

$$C = \log_2 \det (I_m + \sigma.HH^H) \quad (8)$$

where σ is the average signal to noise ratio per receiving antenna; I_m denotes the identity matrix of size *m*, the upper script ^{H} represents the hermitian conjugate of the matrix and

det(X) means the determinant of a matrix X. To clearly point out the MIMO system performance for the LOS and NLOS cases, the ergodic capacity is calculated for a fixed transmitted power and the SNR at the receiver is determined by the path loss. In this case, the capacity includes both effects related to received power and spatial richness. The relationship between the channel capacity C and the distance d_{Tx-Rx} based on equation (8) is shown in figure 18. Obviously, one can see that the NLOS suffer from its higher path-loss exponent which is due to the directional radiation pattern of the MIMO patch antenna resulting in lower capacity compared to the LOS case by about 3 bit/s/Hz.

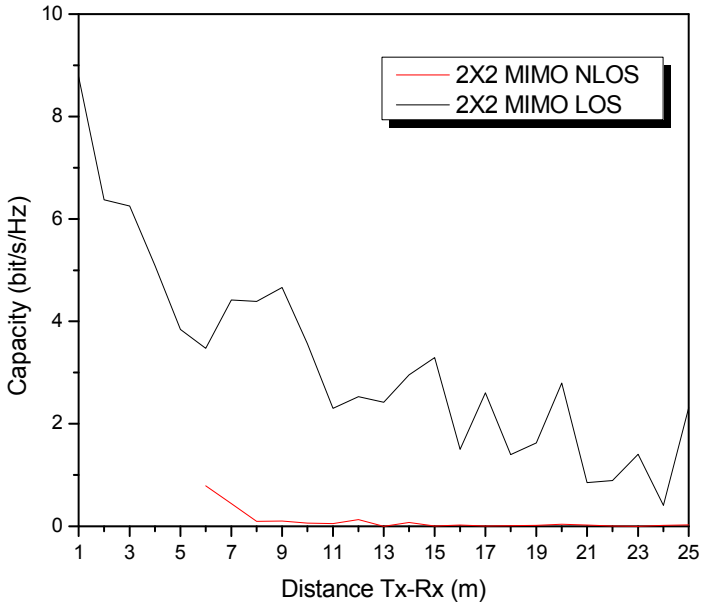

Fig. 18. Channel capacity for LOS and NLOS scenarios

4. Conclusion

This study deals with several aspects relative to UWB and MIMO propagation channel and its deployment for wireless sensors. Successful design and deployment of these techniques require detailed channel characterization. Measurement campaigns, made at two different deep levels in a former gold mine under LOS and NLOS scenarios, have been analyzed to obtain the relevant statistical parameters of the channel.

Although MIMO system can offer high capacity performance through multipath propagation channel but it has some drawbacks such as complexity, power consumption and size limitation of the wireless sensor. However, UWB has several advantages compared to narrowband systems. The wide bandwidth (typically 500 MHz or more) gives UWB excellent immunity to interference from narrowband systems and from multipath effects. Another important benefit of UWB is its high data rate. Additionally, UWB offers significant advantages with respect to robustness, energy consumption and location accuracy.

Nevertheless, UWB technology for wireless networks is not all about advantages. Some of the main difficulties of UWB communication are low transmission power so information can only travel for short distance comparing to 2.4 GHz which can rich long distance. Moreover UWB in the microwave range does not offer a high resistance to shadowing, but this problem can be mitigated in sensor networks by appropriate routing, and possible collaborative communications.

5. References

A. A. M. Saleh and R. A. Valenzuela, "A Statistical Model for Indoor Multipath Propagation," IEEE J. Select. Areas Commun., vol. SAC-5, pp. 128-137, Feb. 1987.

A. F. Molisch, B. Kannan, C. C. Chong, S. Emami, A. Karedal, J. Kunisch, H. Schantz, U. Schuster and K. Siwiak, "IEEE 802.15.4a Channel Model – Final Report", IEEE 802.15-04 0662-00-004a, San Antonio, TX, USA, Nov. 2004.

A.J. Goldsmith S. Cui and A. Bahai.: 'Energy-efficiency of mimo and cooperative mimo in sensor networks', IEEE Journal on Selected Areas of Communications, 22(6), August 2004.

A.Muqaibel, A. Safaai-Jazi, A, Attiya, B Woerner, and S. Riad, "Path-Loss and time dispersion parameters for indoor UWB propagation ", Wireless Communications, IEEE Transactions, Vol 5, Issue 3, March 2006 Pages 550-559.

Arslan A, Chen AN and Benedetto MG (2006) Ultra-wideband wireless communication. Wiley Interscience, Hoboken, New Jersey.

Arslan H and Benedetto MGD (2005) Introduction to UWB. Book Chapter, Ultra Wideband Wireless Communications (ed. Arslan H), John Wiley & Sons, USA.

Chehri A and Fortier P (2006a) Frequency domain analysis of UWB channel propagation in underground mines. Proceedings of IEEE 64th Vehicular Technology Conference, Montreal, Canada, 25–28 September 2006, pp. 1–5.

Chehri A, Fortier P and Tardif PM (2006a) Deployment of ad-hoc sensor networks in underground mines. Proceedings of Conference on Wireless and Optical Communication, and Wireless Sensor Network, Alberta, Canada, 3–4 July 2006, pp. 13–19.

Choi JD and Stark WE (2002) Performance of ultra-wideband communications with suboptimal receivers in multipath channels. IEEE Journal on Selected Areas in Communications, pp. 1754–1766.

F. Granelli, H. Zhang, X. Zhou, S. Maranò, "Research Advances in Cognitive Ultra Wide Band Radio and Their Application to Sensor Networks," Mobile Networks and Applications, Vol. 11, pp. 487-499, 2006.

G. J. Foschini and J. Gans, "On Limits of Wireless Communications in a Fading Environment when Using Multiple Antennas", Wireless Personal Communications, vol. 6, no. 3, pp. 315-335, March, 1996

J. Li, T. Talty, "Channel Characterization for Ultra-Wideband Intra-Vehicle Sensor Networks," Military Communications conference (MILCOM), pp. 1-5, 2006.

L. Stoica, A. Rabbachin, H.O. Repo, T.S. Tiuraniemi, I. Oppermann, "An Ultrawideband System Architecture for Tag Based Wireless Sensor Networks," IEEE Transactions on Vehicular Technology, Vol. 54, pp. 1632-1645, 2005.

L. Yuheng, L. Chao, Y. He, J. Wu, Z. Xiong, "A Perimeter Intrusion Detection System Using Dual-Mode Wireless Sensor Networks," Second International Conference on Communications and Networking in China, pp. 861-865, 2007.

M. Chamchoy, W. Doungdeun, S, Promwong "Measurement and modeling of UWB path loss for single-band and multi-band propagation channel", Communications and Information Technology, 2005. ISCIT 2005. IEEE International Symposium, vol2, 12-14 Oct. 2005 Pages:991-995.

Molisch AF (2005) Ultra wideband propagation channels-theory, measurement, and modeling. IEEE Transactions on Vehicular Technology, pp. 1528–1545.

Molisch, A. F.; Cassioli, D.; Chong, C.-C.; Emami, S.; Fort, A.; Kannan, B.; Karedal, J.; Kunisch, J.; Schantz, H. G.; Siwiak, K.; Win, M. Z.; "A Comprehensive Standardized Model for Ultrawideband Propagation Channels", Antennas and Propagation, IEEE Transactions on. Volume 54, Issue 11, Part 1, Nov. 2006 Page(s):3151 - 3166

Nedil M, Denidni TA, Djaiz A and Habib AM (2008) A new ultra-wideband beamforming for wireless communications in underground mines. Progress in Electromagnetics Research, 4: 1–21.

R.S. Thoma, O. Hirsch, J. Sachs, Zetik, R., "UWB Sensor Networks for Position Location and Imaging of Objects and Environments," The Second European Conference on Antennas and Propagation (EuCAP), pp. 1-9, 2007.

S. Ghassemzadeh, L. Greenstein, T. Sveinsson, A.Kavcic, V. Tarokh, "UWB indoor path loss model for residential and commercial environments," in Proc. IEEE Veh. Technol. Conf (VTC 2003- Fall), Orlando, FL, USA, pp. 629-633, Sept. 2003.

T. S. Rappaport, Wireless Communications: Principles & Practice, Upper Saddle River, NJ, Prentice Hall PTR, 1996

X. Huang, E. Dutkiewicz, R. Gandia, D. Lowe, "Ultra-Wideband Technology for Video Surveillance Sensor Networks," IEEE International Conference on Industrial Informatics, pp. 1012-1017, 2006.

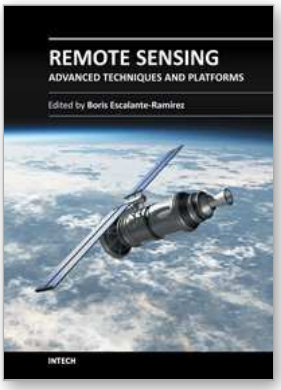

Remote Sensing - Advanced Techniques and Platforms
Edited by Dr. Boris Escalante

ISBN 978-953-51-0652-4
Hard cover, 462 pages
Publisher InTech
Published online 13, June, 2012
Published in print edition June, 2012

This dual conception of remote sensing brought us to the idea of preparing two different books; in addition to the first book which displays recent advances in remote sensing applications, this book is devoted to new techniques for data processing, sensors and platforms. We do not intend this book to cover all aspects of remote sensing techniques and platforms, since it would be an impossible task for a single volume. Instead, we have collected a number of high-quality, original and representative contributions in those areas.

How to reference
In order to correctly reference this scholarly work, feel free to copy and paste the following:

Larbi Talbi, Ismail Ben Mabrouk and Mourad Nedil (2012). Progress Research on Wireless Communication Systems for Underground Mine Sensors, Remote Sensing - Advanced Techniques and Platforms, Dr. Boris Escalante (Ed.), ISBN: 978-953-51-0652-4, InTech, Available from: http://www.intechopen.com/books/remote-sensing-advanced-techniques-and-platforms/progress-research-on-wireless-communication-systems-for-underground-mine-sensors

INTECH
open science | open minds

InTech Europe
University Campus STeP Ri
Slavka Krautzeka 83/A
51000 Rijeka, Croatia
Phone: +385 (51) 770 447
Fax: +385 (51) 686 166
www.intechopen.com

InTech China
Unit 405, Office Block, Hotel Equatorial Shanghai
No.65, Yan An Road (West), Shanghai, 200040, China
中国上海市延安西路65号上海国际贵都大饭店办公楼405单元
Phone: +86-21-62489820
Fax: +86-21-62489821